# Degeneracy and discreteness in cosmological model fitting

Huan-Yu Teng[1], Yuan Huang[1] and Tong-Jie Zhang[1,2,3]

[1] Department of Astronomy, Beijing Normal University, Beijing 100875, China; *tjzhang@bnu.edu.cn*
[2] Departments of Physics and Astronomy, University of California, Berkeley, CA 94720, USA
[3] Lawrence Berkeley National Laboratory, 1 Cyclotron Road, Berkeley, CA 94720, USA

**Abstract** We explore the problems of degeneracy and discreteness in the standard cosmological model (ΛCDM). We use the Observational Hubble Data (OHD) and the type Ia supernovae (SNe Ia) data to study this issue. In order to describe the discreteness in fitting of data, we define a factor $\mathcal{G}$ to test the influence from each single data point and analyze the goodness of $\mathcal{G}$. Our results indicate that a higher absolute value of $\mathcal{G}$ shows a better capability of distinguishing models, which means the parameters are restricted into smaller confidence intervals with a larger figure of merit evaluation. Consequently, we claim that the factor $\mathcal{G}$ is an effective way of model differentiation when using different models to fit the observational data.

**Key words:** cosmological parameters — cosmology: observations — methods: statistical

## 1 INTRODUCTION

The *PLANCK* (Planck Collaboration et al. 2014) satellite released its first results in 2013, which gave tighter constraints on cosmological parameters than before. Extensive observations have been made to constrain cosmological parameters including the Observational Hubble Data (OHD) (Yi & Zhang 2007; Zhang et al. 2014; Ma & Zhang 2011; Moresco et al. 2012; Farooq et al. 2013; Farooq & Ratra 2013; Yuan & Zhang 2015), type Ia supernovae (SNe Ia) (Suzuki et al. 2012; Perlmutter & Schmidt 2003; Riess et al. 1998), cosmic microwave background (CMB) radiation (Dunkley et al. 2009; Komatsu et al. 2011; Hinshaw et al. 2013; Planck Collaboration et al. 2014) and baryon acoustic oscillations (BAO) (Eisenstein et al. 2005; Percival et al. 2010). Qualitatively, the constraints imposed by more numerous observations can provide smaller confidence intervals for cosmological parameters. However, quantitative studies address how well the cosmological parameters are constrained if only a limited number of datasets are available. In this paper, we present a new method that relies on a factor $\mathcal{G}$ to investigate this issue with OHD and SNe Ia data and using the confidence interval and figure of merit (FoM) as evaluation criteria.

## 2 METHODOLOGY

### 2.1 Standard Cosmological Model (ΛCDM)

We examine a standard non-flat ΛCDM model with a curvature term, $\Omega_{\mathrm{k}} = 1 - \Omega_{\mathrm{m}} - \Omega_{\Lambda}$, but without a radiation term (Ma & Zhang 2011; Farooq et al. 2013). Specifically,

the Hubble parameter is given by

$$
\begin{aligned}
H(z) &= H_0 E(z; \Omega_{\mathrm{m}}, \Omega_{\Lambda}, H_0) \\
&= H_0 \sqrt{\Omega_{\mathrm{m}}(1+z)^3 + \Omega_{\mathrm{k}}(1+z)^2 + \Omega_{\Lambda}} \,. \quad (1)
\end{aligned}
$$

The relationship between luminosity distance and redshift of SNe Ia is described as below (Riess et al. 1998; Liu et al. 2011)

$$
D_L = \frac{c(1+z)}{H_0} \mathrm{sinn}\left[\sqrt{|\Omega_{\mathrm{k}}|} \int_0^{z'} \frac{1}{E(z; \Omega_{\mathrm{m}}, \Omega_{\Lambda}, H_0)} dz'\right],
\tag{2}
$$

$$
\mathrm{sinn}(x) = \begin{cases} \sinh x & \Omega_{\mathrm{k}} > 0 \\ x & \Omega_{\mathrm{k}} = 0 \\ \sin x & \Omega_{\mathrm{k}} < 0 \end{cases}.
$$

Noting that $\Omega_{\mathrm{m}} + \Omega_{\Lambda} + \Omega_{\mathrm{k}} = 1$, we have

$$
D_L = \frac{1+z}{|\sqrt{1 - \Omega_{\mathrm{m}} - \Omega_{\Lambda}}|} \mathrm{sinn}[\sqrt{1 - \Omega_m - \Omega_{\Lambda}} \chi(z)],
$$

$$
\chi(z) = \int_0^z \frac{dz'}{E(z; \Omega_{\mathrm{m}}, \Omega_{\Lambda}, H_0)} \,.
\tag{3}
$$

The distance modulus is given by following an empirical equation (Perlmutter et al. 1997)

$$
\mu = 5 \log D_L - 5 \log H + 52.384 \,.
\tag{4}
$$

Combining Equations (3) and (4), we obtain the relationship between distance modulus and redshift, which is dependent upon cosmological parameters.

Two datasets are utilized to constrain cosmological parameters. These are the existing OHD with 28 data points (Zhang et al. 2014; Simon et al. 2005; Stern et al. 2010;

Moresco et al. 2012; Busca et al. 2013; Blake et al. 2012; Chuang & Wang 2013) and the SNe Ia data provided by the Supernova Cosmology Project (SCP) (Suzuki et al. 2012), which contain 580 SNe Ia with redshifts, distance moduli and errors.

## 2.2 Degeneracy and Discreteness

How the Hubble parameter and the distance modulus depend on redshift are shown in Figure 1. An inspection of Figure 1 suggests that in low-redshift regions, different models predict very similar distance moduli, i.e., they are degenerate. Therefore, the OHD and SNe Ia data in low-redshift regions cannot be used to distinguish these models. Here we examine Figure 2 to find the observational error associated with the OHD and SNe Ia datasets since error bars are not clearly shown in Figure 1. From Figure 2, we find that the values of observational errors are basically at the level of the red line, and in the region representing OHD errors are from 0 to 30 while in the region representing SNe Ia errors are from 0.1 to 0.3. In addition,

Figure 2 does not show an obvious relationship between observational error and redshift.

Based upon the likelihood function of a single point, we can study the relationship between the goodness-of-fit and the final fitting results for a given model. With a set of data for fitting, the probability densities of each point show little difference in parameter space, suggesting that the probabilities of all parameters are approximately the same. We cannot distinguish the best fitting points, however the confidence intervals are relatively large. In order to examine the quality of single points, we apply a perturbation to one parameter and investigate how the likelihood of the single point varies. This can be regarded as finding the absolute value of derivative of the likelihood. Likelihood depends on parameters (we give the equations in Sect. 2.3), which indicate that we can calculate the derivative of the likelihood with respect to the parameters.

For the OHD dataset, we calculate the partial derivative of $H(z; \Omega_m, \Omega_\Lambda, H_0)$ with respect to different parameters. In this paper, we do not consider the goodness of confidence intervals for $H_0$.

$$\frac{\partial H}{\partial \Omega_m} = \frac{H_0 z(1+z)^2}{2\sqrt{\Omega_m(1+z)^3 + \Omega_\Lambda + (1-\Omega_m-\Omega_\Lambda)(1+z)^2}}, \tag{5}$$

$$\frac{\partial H}{\partial \Omega_\Lambda} = \frac{-H_0 z(z+2)}{2\sqrt{\Omega_m(1+z)^3 + \Omega_\Lambda + (1-\Omega_m-\Omega_\Lambda)(1+z)^2}}. \tag{6}$$

For the SNe Ia dataset, we calculate the partial derivative of distance modulus with respect to parameters $\mu = \mu(z; \Omega_m, \Omega_\Lambda, H_0)$:

$$\frac{\partial \mu}{\partial \Omega_m} = \frac{5}{\ln 10} \frac{1}{D_L} \left\{ \mathrm{cosn}\left[|\sqrt{\Omega_k}\chi(z)|\right] \left[ -\frac{1}{2}\frac{\chi(z)}{2\Omega_k} - \int_0^z \frac{dz}{2E^3} z(z+1)^2 \right] \right\}, \tag{7}$$

$$\frac{\partial \mu}{\partial \Omega_\Lambda} = \frac{5}{\ln 10} \frac{1}{D_L} \left\{ \frac{D_L}{2\Omega_k} + (1+z)\mathrm{cosn}(|\sqrt{\Omega_k}\chi(z)|) \left[ -\frac{1}{2}\frac{\chi(z)}{2\Omega_k} - \int_0^z \frac{dz}{2E^3} z(z+2) \right] \right\}. \tag{8}$$

Notice that in the above four functions, $\Omega_m + \Omega_\Lambda + \Omega_k = 1$ is still assumed and the definition of $\mathrm{cosn}(x)$ is similar to that of $\mathrm{sinn}(x)$.

$$\mathrm{cosn}(x) = \begin{cases} \cosh x & \Omega_k > 0, \\ x & \Omega_k = 0, \\ \cos x & \Omega_k < 0. \end{cases}$$

## 2.3 Definition of Factor $\mathcal{G}$

In the following equations, we introduce $\theta$ to represent $\Omega_m$ or $\Omega_\Lambda$, and $x$ represents the observational variables, $\mu$ or $H$. For the sake of simplicity, we use the subscripts 'th' to denote theoretical values and 'ob' to denote observational values, i.e $x_{th}$ and $x_{ob}$ respectively. $\mathcal{L}$ is the symbol for

likelihood, i.e.,

$$\mathcal{L}_i(z; \theta|\boldsymbol{x}) = \exp\left[ -\frac{(\boldsymbol{x}_{ob,i} - \boldsymbol{x}_{th,i})^2}{2\sigma_i^2} \right], \tag{9}$$

$$\frac{\partial}{\partial \theta}(-\ln \mathcal{L}_i) = \frac{(\boldsymbol{x}_{ob,i} - \boldsymbol{x}_{th,i})}{\sigma_i^2} \frac{\partial \boldsymbol{x}_{th,i}}{\partial \theta}. \tag{10}$$

The posterior of a model is proportional to the product of the likelihood at each point

$$\frac{\partial}{\partial \theta}(-\ln \mathcal{L}) = \frac{\partial}{\partial \theta}\left( -\ln \prod_{i=1}^n \mathcal{L}_i \right), \tag{11}$$

$$\frac{\partial}{\partial \theta}(-\ln \mathcal{L}) = \frac{\partial \boldsymbol{x}_{th,n}}{\partial \theta} \frac{(\boldsymbol{x}_{ob,n} - \boldsymbol{x}_{th,n})}{\sigma_n^2}$$
$$+ \sum_{i=1}^{n-1} \left[ \frac{\partial \boldsymbol{x}_{th,i}}{\partial \theta} \frac{(\boldsymbol{x}_{ob,i} - \boldsymbol{x}_{th,i})}{\sigma_i^2} \right]. \tag{12}$$
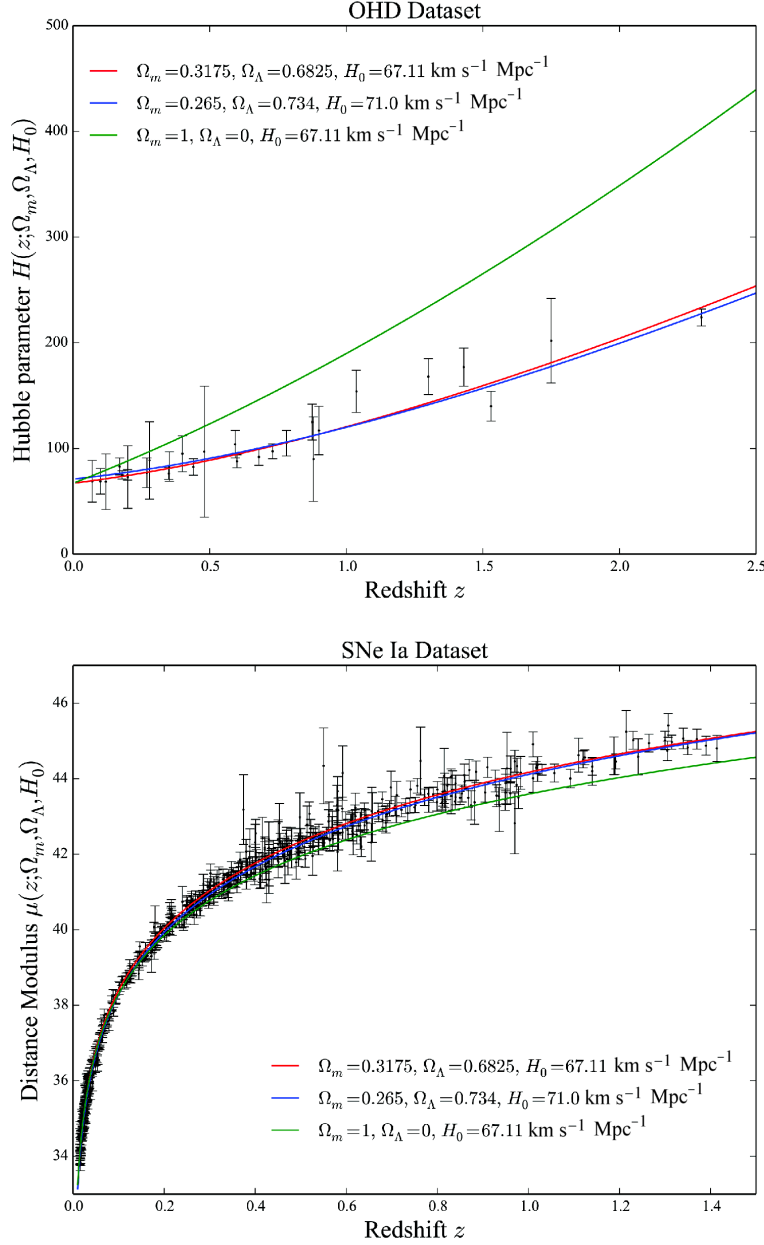
**Fig. 1** Theoretical and observational Hubble parameter and the distance modulus of SNe Ia. The upper panel shows the OHD dataset with $1\sigma$ confidence intervals and the theoretical $H(z; \Omega_{\mathrm{m}}, \Omega_\Lambda, H_0)$ value of different models. The lower one indicates the SNe Ia datasets with $1\sigma$ confidence intervals and the theoretical curves predicted by different models. The red, blue and green curves represent predictions from models associated with the *PLANCK* (Planck Collaboration et al. 2014) and WMAP (Komatsu et al. 2011) data, and the model with only a matter term, respectively. Black dots and error bars indicate observational data.

The observational error is stochastic, representing random differences between $\boldsymbol{x}_{\mathrm{ob},i}$ and $\boldsymbol{x}_{\mathrm{th},i}$. Moreover, only values for the gradient are important for our study. Hence we set $\boldsymbol{x}_{\mathrm{ob},i} - \boldsymbol{x}_{\mathrm{th},i} = \sigma = \bar{\sigma}$, where $\bar{\sigma}$ is the average of observational errors of all data. Under the same conditions, we can define the discreteness factor $\mathcal{G}$ which is proportional to $\frac{1}{\sigma}\frac{\partial \boldsymbol{x}_{\mathrm{th}}}{\partial \theta}$

The factor $\mathcal{G}$ depends on the redshifts and the confidence intervals of the data. Small confidence intervals are required to distinguish models if the models tend to be degenerate. In the parameter regions where the models appear to be discrete, we do not need small confidence intervals. The value of $\mathcal{G}$ can be used to quantitatively measure the discreteness of data points with errors at different redshifts.

$$\mathcal{G}(z; \theta | \boldsymbol{x}) = \frac{1}{\sigma}\frac{\partial \boldsymbol{x}_{\mathrm{th}}}{\partial \theta} \ . \tag{13}$$
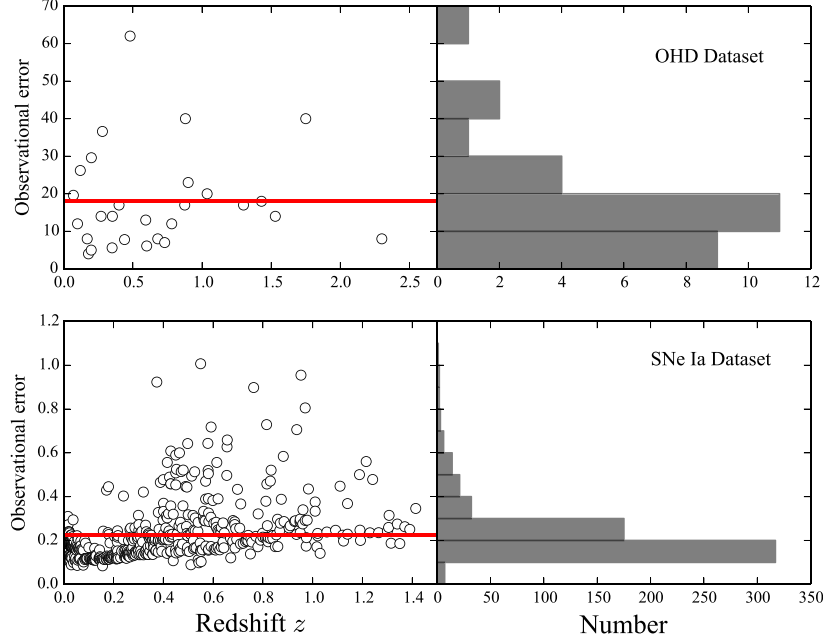
**Fig. 2** The observational error of the SNe Ia dataset given by SCP. The top panels illustrate the OHD dataset and the bottom panels display the SNe Ia datasets. In addition, the left panels show the two dimensional plots of observational error versus redshift, where the red lines are the average values of all errors. The right panels show histograms of the distributions of observational errors (OHD in 10 bins and SNe Ia in 12 bins).

In the fitting process, if a new observational data point is added, it will have an effect on the result such that

$$\mathcal{G}_n = \frac{\partial}{\partial\theta}(-\ln\mathcal{L}_n),\tag{14}$$

$$\frac{\partial}{\partial\theta}(-\ln\mathcal{L}) = \mathcal{G}_n$$
$$+ \sum_{i=1}^{n-1}\left[\frac{\partial\boldsymbol{x}_{\mathrm{th},i}}{\partial\theta}\frac{(\boldsymbol{x}_{\mathrm{ob},i}-\boldsymbol{x}_{\mathrm{th},i})}{\sigma_i^2}\right].\tag{15}$$

Here we use $-\ln\mathcal{L}(z,\theta)$ instead of $\mathcal{L}(z,\theta)$ to simplify the formulas. It is not so important to find an explicit equation for the likelihood. Now we have a criterion to measure the discreteness of different data points caused by the model itself. In the next section, we will apply our method to the existing 28 OHD and 580 SNe Ia data given by SCP to examine the ability of the factor $\mathcal{G}$ to judge the discreteness of data points.

## 3 ANALYSIS AND RESULTS

One of the results that we focus on is the relationship between the redshift $z$ and the factor $\mathcal{G}$. From the definition of the factor $\mathcal{G}$, we find it is also related to the parameters we select, which means, for different parameters at the same redshift, the goodness of discreteness of the data points is different.

Nowadays, constraints on cosmological parameters give the value of $\Omega_{\mathrm{m}} \simeq 0.32$ and $\Omega_{\Lambda} \simeq 0.68$ (Planck

Collaboration et al. 2014), i.e. *PLANCK*. In our experiment, we find that these values are hardly affected by adding more datasets. After parameters are confirmed, the factor $\mathcal{G}$ will be a function that only depends on the redshift and observational error.

Figure 3 shows how factor $\mathcal{G}$ changes with redshift $z$. Here, for the theoretical value of factor $\mathcal{G}$, we assume that all the standard deviations are equal to the average standard deviation. For an observational value of factor $\mathcal{G}$, we take observational standard deviations. Since the key point is the degree that likelihood changes with the cosmological parameter, it is sufficient to focus on the absolute value $|\mathcal{G}|$.

From Figure 3, we find that $|G(z;\Omega_{\mathrm{m}}|\boldsymbol{x})|$ and $|G(z;\Omega_{\Lambda}|H)|$ monotonically increase with redshift, while $|G(z;\Omega_{\Lambda}|\mu)|$ does not, which indicates that for the constraint on $\Omega_{\mathrm{m}}$, high redshift data show an obvious advantage. However, this is not the case for $\Omega_{\Lambda}$, since high redshift datasets of SNe Ia do not show this kind of advantage. Considering the true standard deviations associated with each data point, Figure 3 also indicates the true value of discreteness. Both true and theoretical standard deviations indicate the same tendency, but due to the different errors associated with each data point, there is a fluctuation in goodness of discreteness. Consequently, although some data points are at higher redshifts, the factor $\mathcal{G}$ for these data points may be smaller than $\mathcal{G}$s of lower redshift data points.

Next, we consider different subsets of data depending on the absolute value of factor $\mathcal{G}$ of $\Omega_{\mathrm{m}}$ and $\Omega_{\Lambda}$ for both

**Table 1** The fitting results by considering different subsets of all data depending on $\mathcal{G}$. In columns $\Omega_{\mathrm{m}}$ and $\Omega_{\Lambda}$: (1) Italic text means these points are reasonable in the $\Lambda$CDM model. (2) Normal text means they are unreasonable in the $\Lambda$CDM model. (3) Blanks in $(\Omega_{\mathrm{m}}, \Omega_{\Lambda})$ mean no constraint results due to non-convergence. (4) Results from $(\Omega_{\mathrm{m}}, \Omega_{\Lambda})$ in bold text and the result in the first row of the table are shown in Fig. 4.

| Dataset | $\theta$ | Lev. | Dat. | $\Omega_{\mathrm{m}}$ | $\Omega_{\Lambda}$ | FoM$_{m\Lambda}$ |
|---|---|---|---|---|---|---|
| SNe Ia | | all | 580 | *0.273±0.070* | *0.712±0.117* | 387.18 |
| SNe Ia | $\Omega_{\mathrm{m}}$ | high | 500 | *0.287±0.071* | *0.751±0.126* | 353.54 |
| SNe Ia | $\Omega_{\mathrm{m}}$ | high | 400 | *0.255±0.086* | *0.657±0.187* | 206.13 |
| SNe Ia | $\Omega_{\mathrm{m}}$ | mid | 500 | *0.320±0.120* | *0.788±0.168* | 200.93 |
| SNe Ia | $\Omega_{\mathrm{m}}$ | mid | 400 | *0.279±0.179* | *0.784±0.223* | 109.64 |
| SNe Ia | $\Omega_{\mathrm{m}}$ | low | 500 | *0.222±0.152* | *0.672±0.187* | 142.60 |
| SNe Ia | $\Omega_{\mathrm{m}}$ | low | 400 | –1.097±0.357 | 0.342±0.353 | |
| SNe Ia | $\Omega_{\Lambda}$ | high | 500 | *0.281±0.072* | *0.739±0.127* | 353.54 |
| SNe Ia | $\Omega_{\Lambda}$ | high | 400 | *0.270±0.081* | *0.706±0.169* | 238.91 |
| SNe Ia | $\Omega_{\Lambda}$ | mid | 500 | *0.291±0.079* | *0.778±0.132* | 303.60 |
| SNe Ia | $\Omega_{\Lambda}$ | mid | 400 | *0.320±0.089* | *0.810±0.147* | 210.99 |
| SNe Ia | $\Omega_{\Lambda}$ | low | 500 | *0.307±0.087* | *0.743±0.137* | 244.70 |
| SNe Ia | $\Omega_{\Lambda}$ | low | 400 | *0.245±0.139* | *0.780±0.189* | 126.50 |
| OHD | | all | 28 | ***0.279±0.078*** | ***0.637±0.260*** | ***128.63*** |
| OHD | $\Omega_{\mathrm{m}}$ | high | 22 | *0.280±0.082* | *0.643±0.279* | 125.11 |
| OHD | $\Omega_{\mathrm{m}}$ | high | 16 | *0.271±0.097* | *0.438±0.416* | 78.18 |
| OHD | $\Omega_{\mathrm{m}}$ | mid | 22 | 0.870±0.220 | 1.480±0.369 | |
| OHD | $\Omega_{\mathrm{m}}$ | mid | 16 | 0.779±0.409 | 1.230±0.661 | |
| OHD | $\Omega_{\mathrm{m}}$ | low | 22 | 0.740±0.391 | 1.220±0.610 | |
| OHD | $\Omega_{\mathrm{m}}$ | low | 16 | | | |
| OHD | $\Omega_{\Lambda}$ | high | 22 | ***0.293±0.072*** | ***0.766±0.235*** | ***150.92*** |
| OHD | $\Omega_{\Lambda}$ | high | 16 | –0.202±1.569 | –0.181±2.072 | 100.72 |
| OHD | $\Omega_{\Lambda}$ | mid | 22 | *0.258±0.091* | 0.497±0.422 | 79.31 |
| OHD | $\Omega_{\Lambda}$ | mid | 16 | | | |
| OHD | $\Omega_{\Lambda}$ | low | 22 | | | |
| OHD | $\Omega_{\Lambda}$ | low | 16 | | | |

OHD and SNe Ia data. To make a comparison, we compute different values for the factor $\mathcal{G}$ that correspond to different parameters. For OHD, we take 28, 22 and 16 out of 28 data, while for SNe Ia, we take 580, 500 and 400 out of 580 data. When not all data are selected, we linearly divide data into three levels, representing the high, middle and low $\mathcal{G}$s of all data. Then we employ a Markov Chain Monte Carlo (MCMC) method to resample the best-fitting points and explore the changes in the best-fitting point and associated confidence intervals. We use the publicly available code PyMC (*https://github.com/pymc-devs/pymc*) to perform a full MCMC analysis. The results are listed in Table 1. The results close to *PLANCK* (Planck Collaboration et al. 2014) and WMAP (Komatsu et al. 2011) can be considered reasonable and these reasonable results are also close to results using SNe Ia data and OHD and given by Komatsu et al. (2011); Ma & Zhang (2011); Moresco et al. (2012); Wang et al. (2012); Farooq et al. (2013); Zhang et al. (2014).

Table 1 indicates that if we select the same level of data, for both $\Omega_{\Lambda}$ and $\Omega_{\mathrm{m}}$, the confidence intervals are generally increasing with the quantities of datasets decreasing, suggesting that our factor $\mathcal{G}$ is effective in distinguishing the data in terms of discreteness. However, we find that in some cases the Markov Chains associated with this group of data do not converge, or the fitting yields abnormal results.

Theories of probability and statistics indicate that the goodness-of-fit increases with the amount of observational data. However, in our experiment, we find that the confidence intervals may become smaller when we remove data with a lower factor $\mathcal{G}$. There are two ways to tighten the constraints associated with a dataset, directly checking the standard deviation error of the constrained parameter to examine the constraint on the specified parameter and establishing a quantified FoM to examine the comprehensive effect on both parameters. The FoM can be defined as long as it reasonably rewards a tight fit while punishing a loose one. We apply the definition of a $0.95$ confidence region in a parameter space (Albrecht et al. 2006), which can be calculated by

$$\mathrm{FoM}_{xy} = \frac{\pi}{A} = \frac{1}{\sigma(\theta_x)\sigma(\theta_y)\sqrt{1-\rho_{xy}}}. \qquad (16)$$

Here $\rho_{xy}$ is a correlation coefficient between $\theta_x$ and $\theta_y$ that is related to covariance matrix $\mathbf{C}_{xy} = \sigma(\theta_x)\sigma(\theta_y)\rho_{xy}$. The larger FoM is, the better constraint we get.

Seeing that in the OHD dataset, we have $\sigma = 0.235$ for the case of 22 data points, which is smaller than $\sigma = 0.260$, if we set $\Omega_{\Lambda}$ as the parameter of $\mathcal{G}$, we consider that OHD at $z = 0.48$, $z = 0.88$ and $z = 1.75$ did not have a positive effect altogether in fitting. Therefore, we may remove these points. We also notice that the FoM$_{m\Lambda}$ for the case of 22 data points is larger than the one that
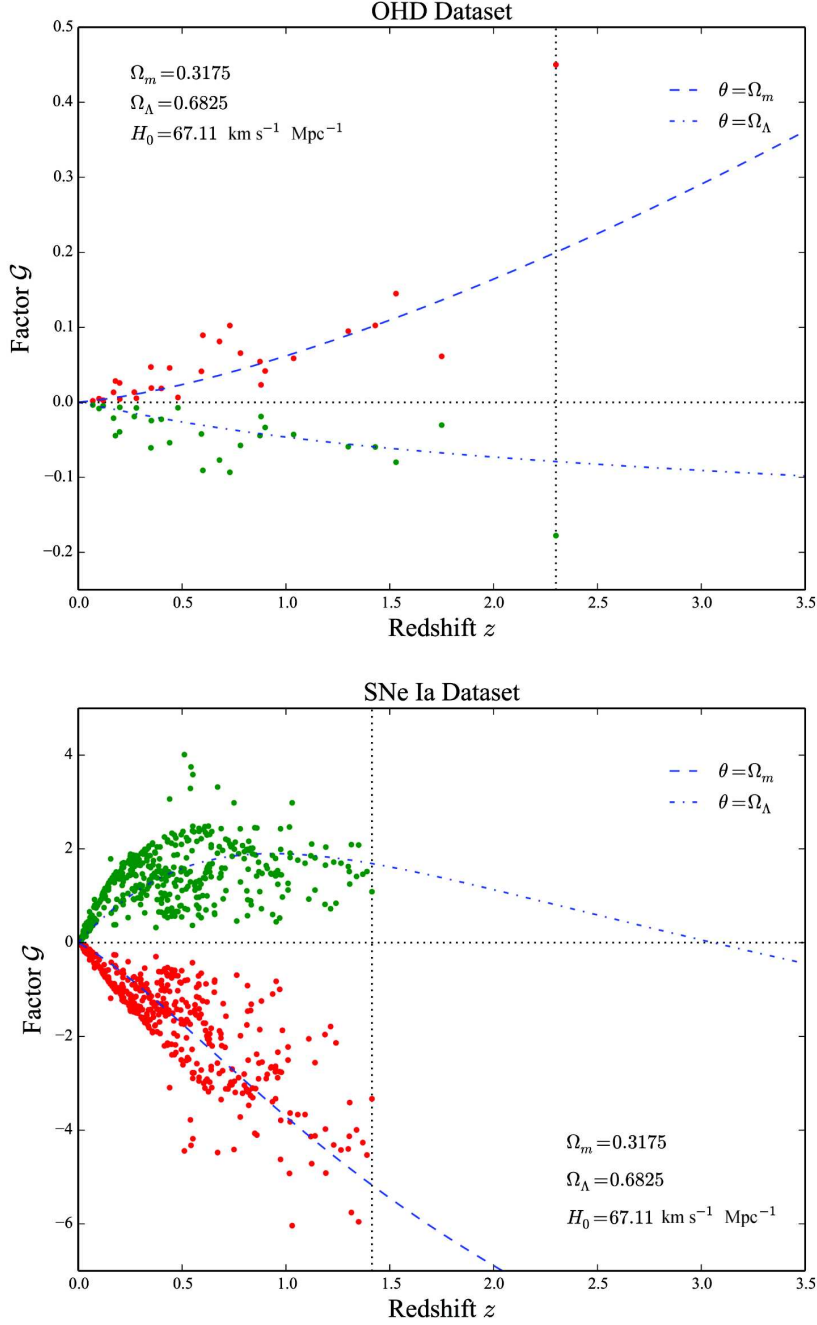
**Fig. 3** Theoretical and observational factor $\mathcal{G}$ of OHD set and SNe Ia dataset. In these two sub-figures, blue dashed and dotted-dashed curves represent the theoretical predictions. We apply the OHD set and SNe Ia dataset in Eq. (13) to calculate factor $G(z; \Omega_m | H)$, $\mathcal{G}(z; \Omega_m | \mu)$, $G(z; \Omega_\Lambda | H)$ and $\mathcal{G}(z; \Omega_\Lambda | \mu)$ of each point, then we plot these $\mathcal{G}$s as dots in the figure. The vertical black dotted line indicates the point of highest redshift and the horizontal black dotted line denotes $\mathcal{G} = 0$.

includes all the data points, which means removing some of the points even improves the total constraint quality.

Moreover, we should notice that the standard deviation associated with $\Omega_m$ and $\Omega_\Lambda$ contains a correlation due to the same $\sigma^{-1}$. Here, a point of larger discreteness of $\Omega_m$ may show a relatively larger discreteness of $\Omega_\Lambda$.

We should mention that the $\mathcal{G}$ factor applies for one parameter in one function, and the effect brought by data removal has been ignored. It can be considered that the factor $\mathcal{G}$ we defined reflects the quality of the observational data. We remove some data in order to investigate how the factor $\mathcal{G}$ changes and find data that do not have a positive effect on the fitted cosmological model. Furthermore, we
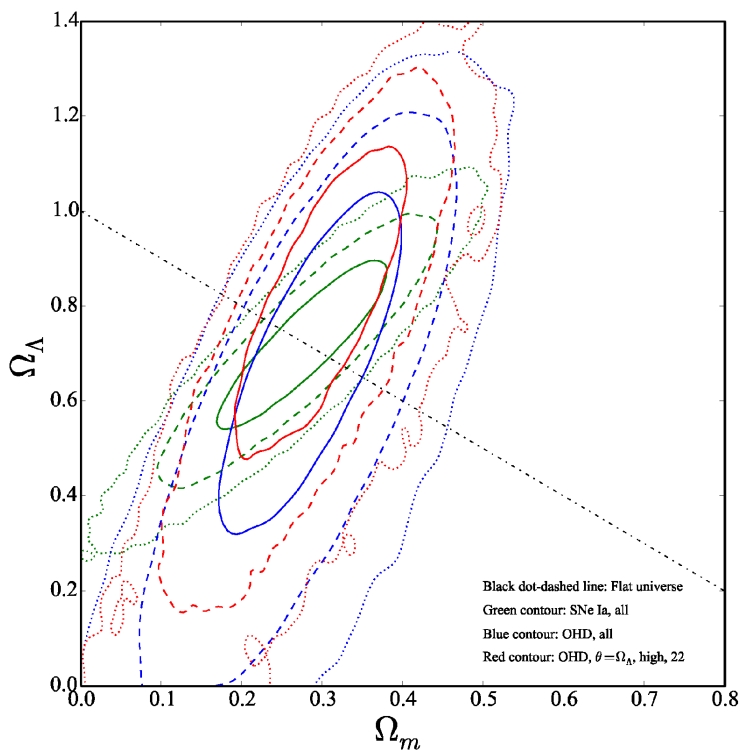
**Fig. 4** Typical confidence regions in the $(\Omega_\Lambda, \Omega_m)$ parameter subspace. The solid, dashed and dotted contours respectively correspond to $68.3\%$, $95.4\%$ and $99.7\%$ intervals. The black dot-dashed line indicates a flat universe. The $\Omega_\Lambda$ interval shown by a red contour is slightly smaller than that shown by a blue contour which is written in bold in Table 1.

deal with these removed points in accordance with specific conditions.

## 4 CONCLUSIONS AND DISCUSSION

In this paper, we develop a new method to study the degeneracy and discreteness in a cosmological model. We define a criterion called discreteness factor $\mathcal{G}$ that relates the modeling functions to likelihood and undetermined parameters. The definition of the factor $\mathcal{G}$ is independent of any specific modeling functions, hence it can be generalized to an arbitrary modeling process. We start from a non-flat $\Lambda$CDM model based on the existing OHD with 28 data points (Zhang et al. 2014; Simon et al. 2005; Stern et al. 2010; Moresco et al. 2012; Busca et al. 2013; Blake et al. 2012; Chuang & Wang 2013) and SNe Ia data with 580 data points released by the SCP (Suzuki et al. 2012). The functions indicate that, theoretically, the factor $\mathcal{G}$ of $\Omega_m$ increases with redshift, however, due to the different observational standard deviations for all data, the true value of $\mathcal{G}$s only shows the trend, especially for the OHD dataset.

We compute the factor $\mathcal{G}$ for $\Omega_m$ and $\Omega_\Lambda$ and consider different subsets of the data utilizing the true value of $\mathcal{G}$s in both the OHD and SNe Ia datasets. We generate an MCMC to find the best-fitting points and their confidence intervals. The fitting results demonstrate that the $\mathcal{G}$ has an effect on the fitting, and a higher absolute value of $\mathcal{G}$ gives a stronger constraint and a larger FoM evaluation. In addition, data with lower $\mathcal{G}$ values may provide not only larger confi-

dence intervals but also unreasonable best-fitting points. However, if the effect of $\mathcal{G}$ is strong enough, it will represent the intrinsic properties of statistics and probability associated with the data. Once we find that the intervals decrease or FoM increases with fewer data that have a lower $\mathcal{G}$ value, we can investigate how observational data affect the associated constraints.

## References

Albrecht, A., Bernstein, G., Cahn, R., et al. 2006, astro-ph/0609591
Blake, C., Brough, S., Colless, M., et al. 2012, MNRAS, 425, 405
Busca, N. G., Delubac, T., Rich, J., et al. 2013, A&A, 552, A96
Chuang, C.-H., & Wang, Y. 2013, MNRAS, 435, 255
Dunkley, J., Komatsu, E., Nolta, M. R., et al. 2009, ApJS, 180, 306

Eisenstein, D. J., Zehavi, I., Hogg, D. W., et al. 2005, ApJ, 633, 560

Farooq, O., Crandall, S., & Ratra, B. 2013, Physics Letters B, 726, 72

Farooq, O., & Ratra, B. 2013, ApJ, 766, L7

Hinshaw, G., Larson, D., Komatsu, E., et al. 2013, ApJS, 208, 19

Komatsu, E., Smith, K. M., Dunkley, J., et al. 2011, ApJS, 192, 18

Liu, D.-Z., Ma, C., Zhang, T.-J., & Yang, Z. 2011, MNRAS, 412, 2685

Ma, C., & Zhang, T.-J. 2011, ApJ, 730, 74

Moresco, M., Verde, L., Pozzetti, L., Jimenez, R., & Cimatti, A. 2012, J. Cosmol. Astropart. Phys., 7, 53

Percival, W. J., Reid, B. A., Eisenstein, D. J., et al. 2010, MNRAS, 401, 2148

Perlmutter, S., & Schmidt, B. P. 2003, in Lecture Notes in Physics, Berlin Springer Verlag, 598, Supernovae and Gamma-Ray Bursters, ed. K. Weiler, 195

Perlmutter, S., Gabi, S., Goldhaber, G., et al. 1997, ApJ, 483, 565

Planck Collaboration, Ade, P. A. R., Aghanim, N., et al. 2014, A&A, 571, A16

Riess, A. G., Filippenko, A. V., Challis, P., et al. 1998, AJ, 116, 1009

Simon, J., Verde, L., & Jimenez, R. 2005, Phys. Rev. D, 71, 123001

Stern, D., Jimenez, R., Verde, L., Kamionkowski, M., & Stanford, S. A. 2010, J. Cosmol. Astropart. Phys., 2, 8

Suzuki, N., Rubin, D., Lidman, C., et al. 2012, ApJ, 746, 85

Wang, X., Meng, X.-L., Zhang, T.-J., et al. 2012, J. Cosmol. Astropart. Phys., 11, 18

Yi, Z.-L., & Zhang, T.-J. 2007, Modern Physics Letters A, 22, 41

Yuan, S., & Zhang, T.-J. 2015, J. Cosmol. Astropart. Phys., 2, 25

Zhang, C., Zhang, H., Yuan, S., et al. 2014, RAA (Research in Astronomy and Astrophysics), 14, 1221